

Low-Temperature Cofired Ceramic LC Filters for RF Applications

■ Lap K. Yeung, Ke-Li Wu, and Yuanxun E. Wang

The latest wireless products demand ever-greater functionality, higher performance, and lower cost in smaller and lighter formats. This demand has been satisfied to date by major advances in integrated circuits and high-density packaging technologies, even though the RF sections have been continuing to demand high-performance and miniaturized passive components such as matching and filtering circuitries. Continuing reductions in the size of discrete surface-mounted components are having diminishing returns because of the incompatibility of printed circuit board (PCB) technology as well as the high cost of assembly for those tiny discrete components. Therefore, new technological approaches are required to address the integration of passives. One of the important means today for integrating passives, particularly for RF functions, is low temperature cofired ceramics (LTCCs). Besides the use of this technology for highly integrated RF front-end modules [1]–[4], there has also been a great deal of interest in realizing compact LTCC-embedded or isolated components, ranging from traditional baluns [5], couplers [6], and filters [7]–[10] to more sophisticated diplexers [11] and balanced filters [12]–[13], for different wireless communication technologies such as mobile phones, Bluetooth, and/or wireless LAN (WLAN) equipped terminals. This article specifically focuses on the design and implementation details for lumped or semi-lumped LTCC bandpass filters.

A variety of LTCC chip-type filters with different characteristics are widely available commercially. They are often specified by the center frequency, fractional bandwidth, insertion loss, and stopband attenuation. Some examples are given in Table 1. These filters are usually second-order or third-order and have their responses optimized for specific applications by taking advantage of flexible filtering characteristics of LTCC LC filters. In general, their design process starts with a schematic circuit usually obtained by computer-aided design techniques from which a physical layout realization

is generated through electromagnetic (EM) simulation tools. Nevertheless, the conventional analytical design methods can always be used as a starting point in the design process. The general design procedure for an LTCC filter can be summarized as

- derive a schematic circuit including parasitic elements
- optimize the circuit to meet required specifications
- generate a physical layout based on the circuit
- tune the layout to meet required specifications
- fabricate prototypes to verify the performance.

Each of these steps has its own design aspects and should be addressed carefully. Generally, layout tuning is the most time-consuming step as it involves full-wave EM simulations. Therefore, having a good layout design to minimize the number of simulations is of primary concern. As miniaturized LTCC filters are usually second-order or third-order, their layouts should not be too complicated. Indeed, there are some well-known standard layout strategies that are commonly used in practice. In the following section, we will discuss some important issues for the whole design process.

Filter Topologies

Having a good schematic circuit is a key step for the successful design of a miniaturized LTCC filter. In this aspect, conventional coupled-resonator filters are promising candidates as they have simple and clear schematics that can be easily translated to multilayer physical layouts. The shunted resonators in these filters are commonly realized by capacitor-loaded quarter-wavelength striplines that can be very compact in size. A general circuit schematic for the coupled-resonator filter is shown in Figure 1. It is seen that between every resonator pair is an admittance inverter that can be considered as a coupling mechanism. In addition, there are also admittance inverters at the two input/output ends of the circuit for impedance transformation purpose. These inverters are usually realized by a π -type network consisting of only capacitors, but other network configurations with only inductors or both inductors and capacitors may also be used. Notice that an L-type network is used instead at the two input/output ends.

A conventional systematic design procedure for this type of filter is given in [14]. The first step in a design is to choose a suitable set of prototype values g_i from the lookup tables based on the desired specifications including return loss, stopband attenuation, and passband ripples. Then, the component values of the resonators are calculated according to

Lap K. Yeung is with the Electrical Engineering Department, University of California, Los Angeles, California, USA.

Ke-Li Wu (klwu@ee.cuhk.edu.hk) is with the Department of Electronic Engineering, The Chinese University of Hong Kong.

Yuanxun E. Wang is with the Electrical Engineering Department, University of California, Los Angeles.

Digital Object Identifier 10.1109/MMM.2008.927634

TABLE 1. Specifications for some typical commercial LTCC chip-type filters.

Frequency (f_0) (MHz)	Bandwidth (MHz)	Insertion Loss (dB)	Attenuation I (dB)	Attenuation II (dB)
1,890	$f_0 \pm 10$	0.8 max	29.0 min @ 1,416–1,437 MHz	22.0 min @ 900 MHz
1,906	$f_0 \pm 14$	1.0 max	38.0 min @ 1,405–1,440 MHz	12.0 min @ 1,649–1,680 MHz
2,450	$f_0 \pm 50$	2.2 max	24.5 min @ 880–960 MHz	12.5 min @ 1,710–1,990 MHz
2,450	$f_0 \pm 50$	1.5 max	25.0 min @ 1200–1,300MHz	10.0 min @ 2,000 MHz
5,820	$f_0 \pm 30$	2.0 max	35.0 min @ 2,000 MHz	30.0 min @ 3,000 MHz

the operating center frequency $\omega_0 = 1/\sqrt{LC}$. The admittance inverters can then be obtained by

$$\begin{aligned} J_{01} &= \sqrt{\frac{Y_0 b_1 \Delta}{g_0 g_1}} \\ J_{j,j+1} &= \Delta \sqrt{\frac{b_j b_{j+1}}{g_j g_{j+1}}}, \quad j = 1, \dots, n-1 \\ J_{n,n+1} &= \sqrt{\frac{Y_0 b_n \Delta}{g_n g_{n+1}}}, \end{aligned} \quad (1)$$

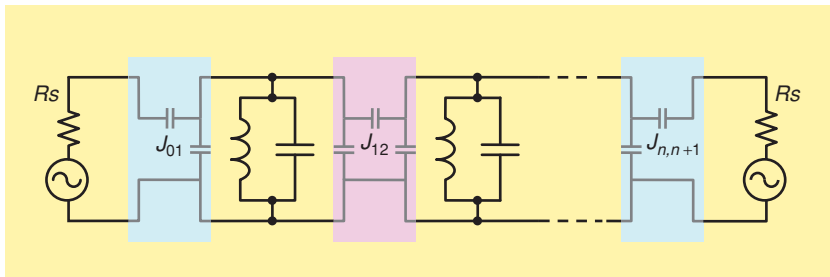
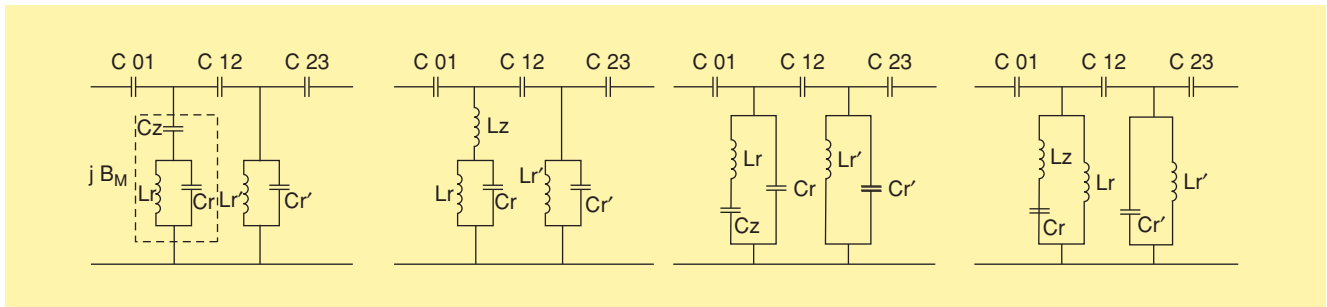
where b_i is the resonator susceptance slope parameter and Δ is the filter fractional bandwidth. However, filters designed by this standard procedure have no transmission zeros and a high-order filter is necessary for having sharp stopband roll-off. Modifications on the inverters can enhance the rejection

characteristics by introducing transmission zeros at the stopband. For example, instead of using capacitor-only π -type networks for the inverters, one of the inverters in Figure 1 can have its series capacitor replaced by a parallel resonant tank so as to create a transmission zero [13] at a prescribed frequency. An important point here is to keep the modified inverter having the same $J_{j,j+1}$ value. Alternatively, adding extra capacitive or inductive elements to the resonators [15]–[16] (see Figure 2) or using shorting stubs [17] can also improve the stopband characteristics. These design methods are essentially the same provided that the modified resonators have the same characteristics as their original counterparts with

$$\begin{aligned} B_m(\omega_z) &= \infty \\ B_m(\omega_0) &= B_o(\omega_0) \\ B_m(\omega_0) &= B'_o(\omega_0), \end{aligned} \quad (2)$$

where B_m and B_o are susceptances of the modified and original resonators, respectively. On the other hand, a more powerful approach is to use computer-based circuit optimization techniques. This approach is always beneficial for designing filters having flexible passband and stopband characteristics. In this case, the standard procedure could serve as the starting point of the optimization process.

Figure 3 depicts several commonly used filter topologies based on the coupled-resonator configuration with either second- or third-order characteristics. The graphs associating with them are their typical


Figure 1. A general coupled-resonator bandpass filter schematic.

Figure 2. Filters with modified resonators for enhanced stopband characteristics.

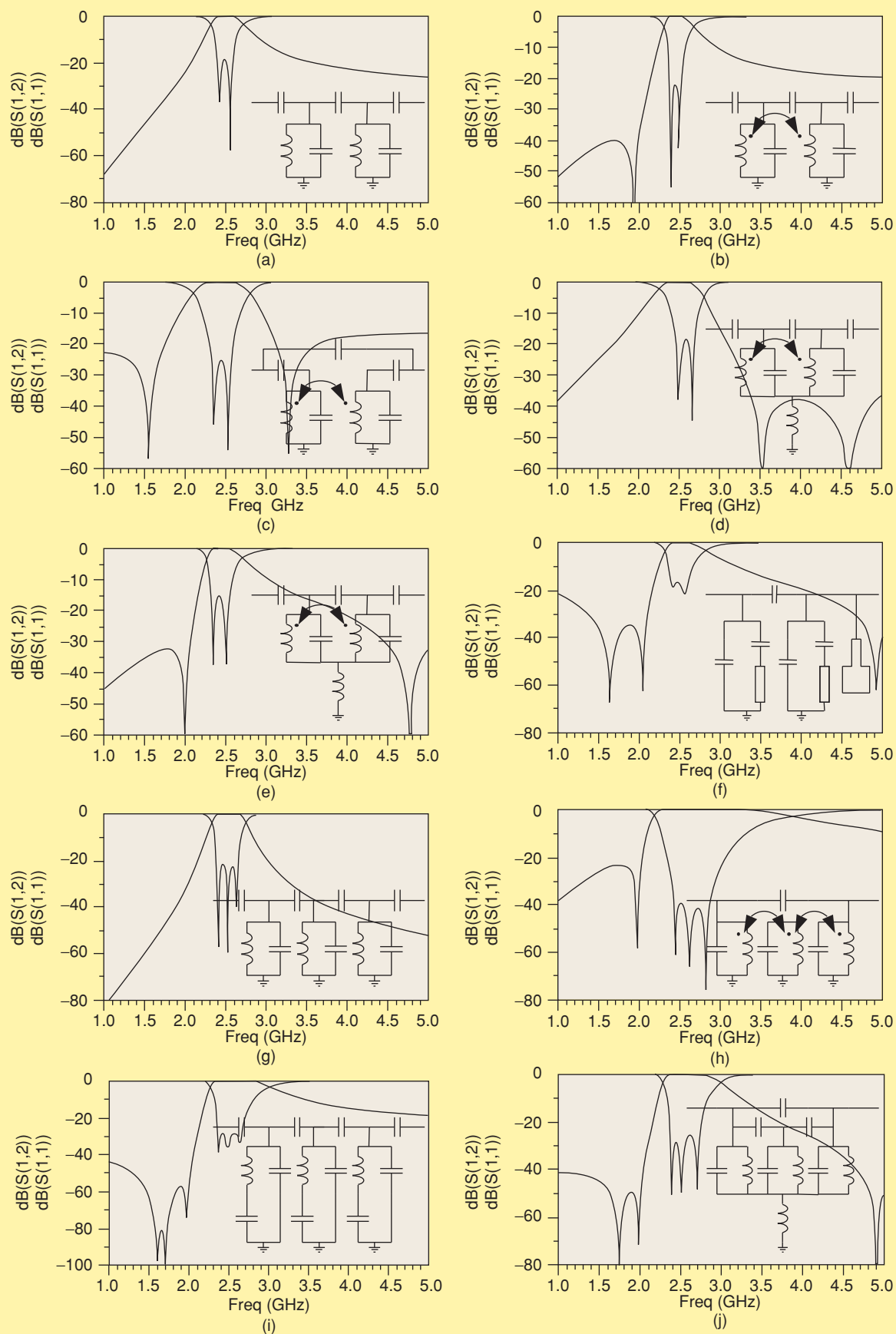


Figure 3. Commonly used coupled-resonator filter topologies and their typical responses.

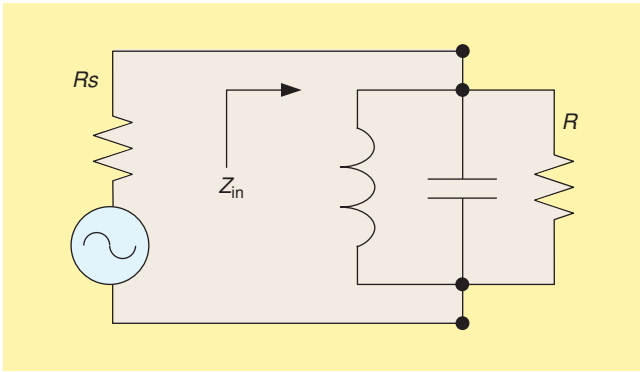


Figure 4. A parallel RLC resonant circuit.

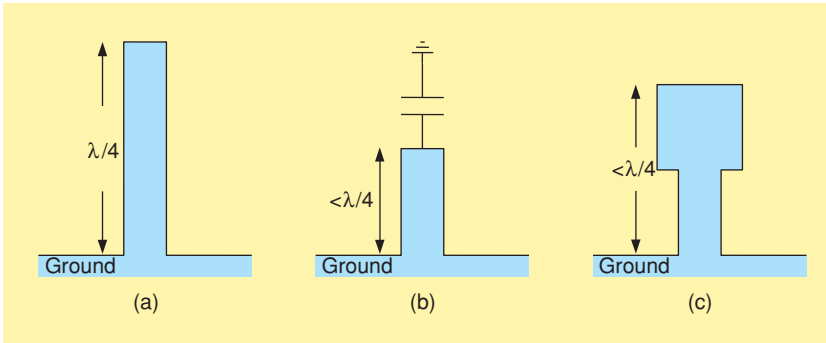


Figure 5. Different transmission-line resonator configurations: (a) a quarter-wave-length resonator; (b) a capacitor-loaded transmission-line resonator; and (c) a stepped-impedance resonator.

S-parameter responses that are obtained by computer optimization. Filters (a) and (g) are the standard filters with no transmission zero. They can be designed analytically by the systematic procedure described previously. As seen in Figure 3(g), the third-order filter has a wider bandwidth and sharper stopband roll-off as compared to the second-order filter shown in Figure 3(a). Filters (b), (d), and (e) all have made use of a modified inverter to introduce a transmission zero at a desired frequency. In addition, (d) and (e) have made use of a grounded inductance to create another transmission zero in the upper stopband. The inductance can be introduced by a short via hole either internally or externally. Filters (c), (h), and (j), on the other hand, have one or more transmission zeros created by a feedback or input/output coupling mechanism. Filter (j) has also used the grounded inductance for an extra zero. Finally, filters (f) and (i) have their resonators modified to achieve enhanced stopband characteristics, and the latter has also contained an extracted-pole resonator using a shorting stub at one of the input/output ends. Notice that (f), (h), and (j) are not as generic as the other filters in the sense that they do not contain any input/output inverters for impedance transformation purpose. Therefore, they may not always have a good return loss for different port impedances. The examples given here are by no means a complete list; they are given merely to indicate the ways to modify the standard coupled-resonator filter configuration to obtain better stopband characteristics.

Resonator Configurations

As noticed in all of the above schematics, the shunted parallel resonator plays a key role in coupled-resonator filters. It determines the passband center frequency and the corresponding insertion loss. Figure 4 shows the lumped-element representation of a parallel resonator. When close to the resonant frequency, the tank has an input impedance of

$$Z_{in}(\omega_0 + \Delta\omega) \approx \frac{R}{1 + j2Q\Delta\omega/\omega_0}, \quad Q = \omega_0 RC, \quad (3)$$

where $\Delta\omega$ is the change of frequency relative to ω_0 . The resistor R includes both the conductor loss in the inductor and dielectric loss in the capacitor. For an LTCC filter, the conductor loss is often more dominant than the dielectric loss in the RF range. Therefore, the design of high- Q inductors is very important as it has significant influence on the passband insertion loss.

It is very helpful to express the resonator's susceptance slope parameter in terms of its inductor and capacitor component values so as to use in (1) directly. The slope parameter is defined as

$$b_r = \left. \frac{\omega_0}{2} \frac{dB_r(\omega)}{d\omega} \right|_{\omega_0}, \quad (4)$$

where B_r is the susceptance of the resonator of interest. Now by using both (3) and (4), we can obtain the relationship between

them as

$$C = \frac{b_r}{\omega_0}, \quad L = \frac{1}{\omega_0 b_r}. \quad (5)$$

There are many ways to realize a parallel resonant circuit in an LTCC filter. However, stepped-impedance and capacitor-loaded quarter-wavelength transmission-line resonators are the two most commonly used configurations. Transmission-line resonators have good quality factors but their sizes are usually large. For example, the shortest transmission-line resonator is the quarter-wavelength line shown in Figure 5. It is short-circuited at one end and open-circuited at the other. It has a parallel type of resonance and can be used for realizing the shunted parallel RLC tanks shown in Figure 4. Assuming the transmission-line implementing a quarter-wavelength line has small loss, when close to the resonant frequency, the input impedance of this resonator has an expression of

$$Z_{in}(\omega_0 + \Delta\omega) \approx \frac{Z_0}{\alpha l + j\pi \Delta\omega/2\omega_0}, \quad (6)$$

where α is the real part of the transmission-line propagation constant and Z_0 is its characteristic impedance. In addition, the quality factor in this case is given by

$$Q = \frac{\beta}{2\alpha}, \quad (7)$$

where β is the imaginary part of the transmission-line propagation constant. Notice that the transmission-line is almost always implemented in stripline format due to its well-shielded property by sandwiching between two ground planes. Although it has the shortest length among different transmission-line resonators, the quarter-wavelength resonator is still not practical to be used directly in miniaturized LTCC filters. In practice, it can be made shorter by having its open end loaded with a shunted capacitor. Alternatively, a stepped-impedance approach [18], as also shown in Figure 5, can be applied. Depending on the value of the loading capacitor or the impedance ratio, the line length can be reduced to as short as one-tenth of the wavelength while still having an acceptable Q factor. It should be pointed out that the capacitor-loaded quarter-wave resonator has the lowest Q factor compared with the stepped-impedance and original quarter-wavelength resonators. An example filter using capacitor-loaded resonators is shown in Figure 6. This is a second-order filter and has the circuit topology of Figure 3(c). Notice how the two resonators are implemented in the layout. The large conducting plate at the end of each line forms a shunted capacitor with the bottom ground plate. The other end is shorted to the ground by a via hole. One of the resonators has its loading capacitor and strips printed in the same layer, and this can in fact be considered as a stepped-impedance resonator (SIR).

Coupling Mechanisms

The coupling mechanism between two resonators is done in the form of an admittance inverter as shown in Figure 1. Depending on the inverter configuration, the coupling can be either capacitive or inductive. Schematics for both inverter types are shown in Figure 7. The inductive π -network can be further transformed to a pair of mutually coupled inductors. This transformation usually results in size reduction as the implementation of a relatively large-size series inductor can be eliminated. The geometry of two broadsided-coupled conducting strips, which are used to provide the necessary mutual inductance, is also depicted in Figure 7. The coupling strength can be controlled by adjusting the horizontal separation distance. As an illustration, the mutual inductance between two conducting strips with a normalized vertical separation (H/W) of 0.48 has been calculated based on (8) with its parameters defined in Figure 8. This formula is derived from the quasi-static assumption [19] and thus works only at low frequency. Notice that the coupling is strongest when one conducting strip is right on top of the other and gradually decreases when they are moving away. In addition, the larger the length-to-width ratio, the stronger the mutual

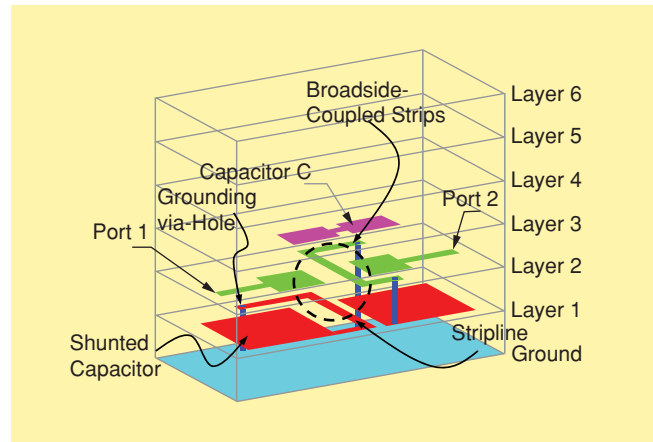


Figure 6. An example second-order filter with capacitor-loaded resonators.

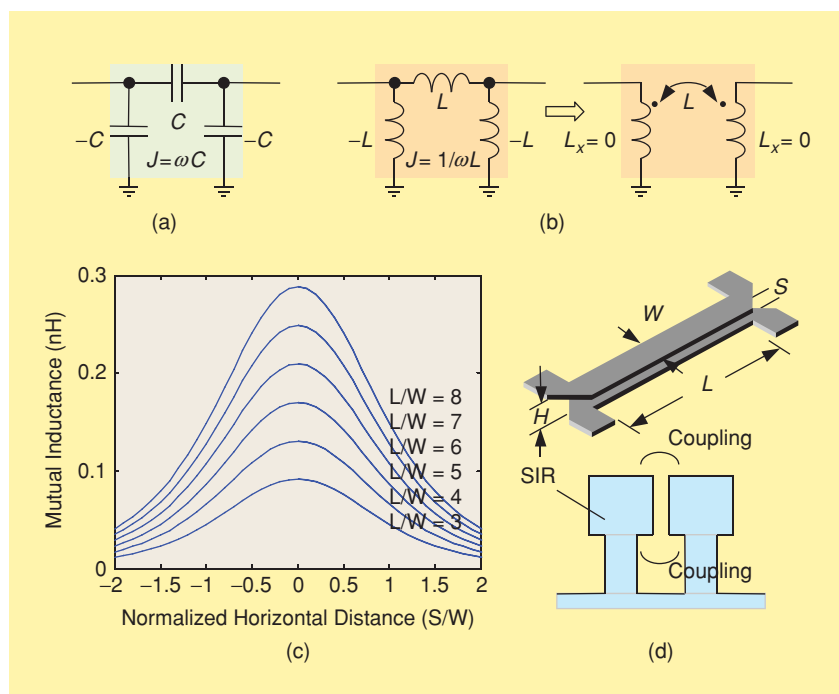


Figure 7. Different resonator-to-resonator coupling mechanisms: (a) a capacitive π -network; (b) inductive π -network; and (c) broadsided- and edge-coupling configurations.

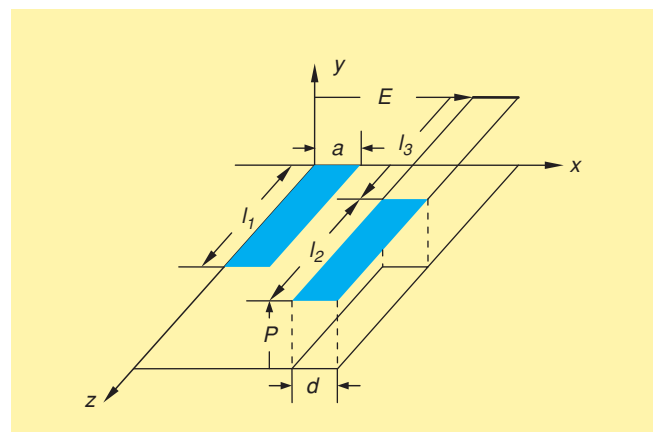


Figure 8. The geometry for two coupled rectangular strips.

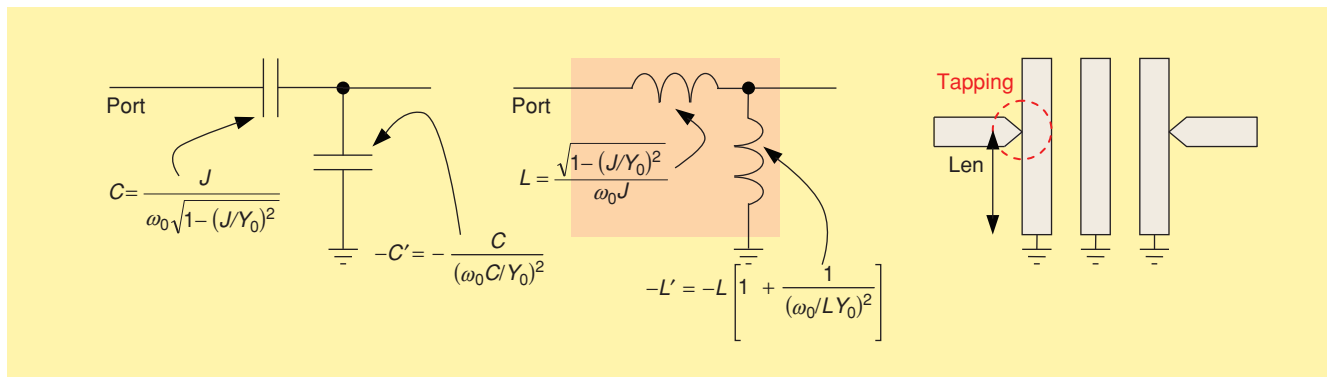


Figure 9. Different input/output coupling mechanisms.

coupling. Alternatively, the edge-coupled configuration can be used if strong coupling is not required.

$$M = \frac{\mu}{4\pi ad} \left[\left[\frac{x^2 - P^2}{2} z \ln \left(z + \sqrt{x^2 + P^2 + z^2} \right) + \frac{z^2 - P^2}{2} x \ln \left(x + \sqrt{x^2 + P^2 + z^2} \right) - \frac{1}{6} (x^2 - 2P^2 + z^2) \sqrt{x^2 + P^2 + z^2} - xPz \tan^{-1} \frac{xz}{P\sqrt{x^2 + P^2 + z^2}} \right]_{E+d-a, E}^{E-a, E+d} \right]_{l_3+l_2-l_1, l_3}^{l_3-l_1, l_3+l_2} (x) (z). \quad (8)$$

On the other hand, capacitance can be approximated by using the well-known parallel-plate formula $C = \epsilon A/d$. Notice that the formulae given here to estimate self- or mutual inductance and capacitance are approximation only. More accurate estimation can be done by using a full-wave EM solver to model a particular coupling structure before incorporating it into an overall filter layout.

For input/output ports, the inverter takes a different form where an L-network is used instead of a π -network (see Figure 9). The details to calculate its component values will be given in the next section. In some filter configurations, a tapping technique can be used for input/output coupling. In such a case, the tapping point location would be very critical as it determines the input/output inverter value.

A Design Example

We are now ready to put everything together by studying a practical design example of a bandpass filter for 2.4-GHz WLAN applications. Required specifications for the filter are listed in Table 2. According to these requirements, the filter should have a center frequency of 2.45 GHz with an operating bandwidth of at least 100 MHz. In addition, its passband return loss should be greater than 15 dB. Normally, a standard third-order filter like the one shown in Figure 3(g) can meet the requirements if the size is not a major concern. However, a second-order filter with a transmission zero at the upper stopband would be a better choice. This transmission zero is used to enhance the stopband rejection at high frequency. Figure 10 shows the proposed schematic. It is essentially a standard configuration consisting of two capacitor-loaded transmission-line resonators and three capacitive inverters.

TABLE 2. Bandpass filter specifications.

Specification	Minimum	Typical	Maximum
Frequency (MHz)	2,400		2,500
Insertion Loss (dB)		1.8	2.2
VSWR (in/out)		1.4	
Attenuation: 902–928 MHz (dB)	58		
Attenuation: 1,850–1,910 MHz (dB)	24		27
Attenuation: 2,000–2,170 MHz (dB)	8		18
Attenuation: 3,400 MHz–3,500 MHz (dB)	15		18
Attenuation 4800 MHz–5000 MHz (dB)	26		29
Attenuation 7200 MHz–7500 MHz (dB)	22		27
Power Rating (W)			4
Ripple (dB)		0.3	0.5

There are small-value inductors attaching at the ground of the loading capacitors to create a transmission zero. The inductance can be a resulting effect from the grounding via holes so that no extra components are necessary. To design this filter, we first proceed to obtain its initial component values by the conventional analytical procedure. The circuit schematic is then further optimized to meet all desired specifications. After that, an initial physical layout is generated based on the optimized circuit schematic. Finally, full-wave EM modeling and tuning are carried out to finalize the layout whose responses should meet all desired specifications. Notice that the responses of the fully tuned layout do not have to exactly match those from the circuit-based simulation.

In this design, the g_i values that give a passband ripple of 0.5 dB are: $g_0 = 1$, $g_1 = 1.4029$, $g_2 = 0.7071$, and $g_3 = 1.9841$. Now we choose the value of L_r to be 1.2 nH, which is a reasonable value for LTCC implementation, and C_r should thus be 3.5 pF for a resonant frequency of 2.45 GHz. Using (1), the values for the three admittance inverters can be obtained as $J_{01} = 0.0125$, $J_{12} = 0.0111$, and $J_{23} = 0.0125$ with the fact that the susceptance slope parameter is given by

$$b_i = \frac{\omega_0}{2} \frac{B_i(\omega_0 + \Delta\omega) - B_i(\omega_0)}{\Delta\omega} = \omega_0 C_r, \quad i = 1 \text{ or } 2, \quad (9)$$

which is same as (4). And in turn, the inverters can be represented by the capacitive L-network and π -network as shown in Figure 10. Their corresponding component values are given by

$$\begin{aligned} C_{01} &= \frac{J_{01}}{\omega_0 \sqrt{1 - (J_{01}/Y_0)^2}} = 1.05 \text{ pF} \\ C'_{01} &= \frac{C_{01}}{1 + (\omega_0 C_{01}/Y_0)^2} = 0.63 \text{ pF} \\ C_{12} &= \frac{J_{12}}{\omega_0} = 0.72 \text{ pF} \\ C_{23} &= \frac{J_{23}}{\omega_0 \sqrt{1 - (J_{23}/Y_0)^2}} = 1.05 \text{ pF} \\ C'_{23} &= \frac{C_{23}}{1 + (\omega_0 C_{23}/Y_0)^2} = 0.63 \text{ pF}, \end{aligned}$$

where the relationships between J and C given in Figure 7 and Figure 9 have been used. For the 1.2-nH inductor, it can be realized by a 33- Ω transmission line with electrical length as

$$\theta = \tan^{-1} \frac{\omega_0 L}{Z_0} = 29.2^\circ.$$

Notice that the 33- Ω characteristic impedance is just a particular selection; different values may be used subjecting to

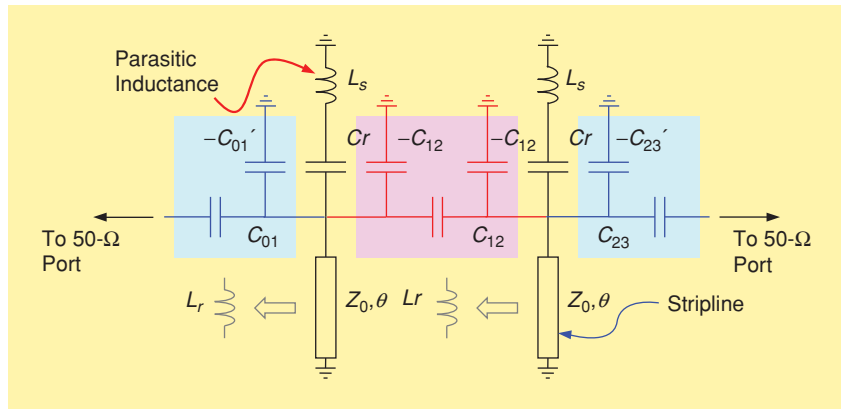


Figure 10. The proposed second-order filter for 2.45-GHz WLAN applications.

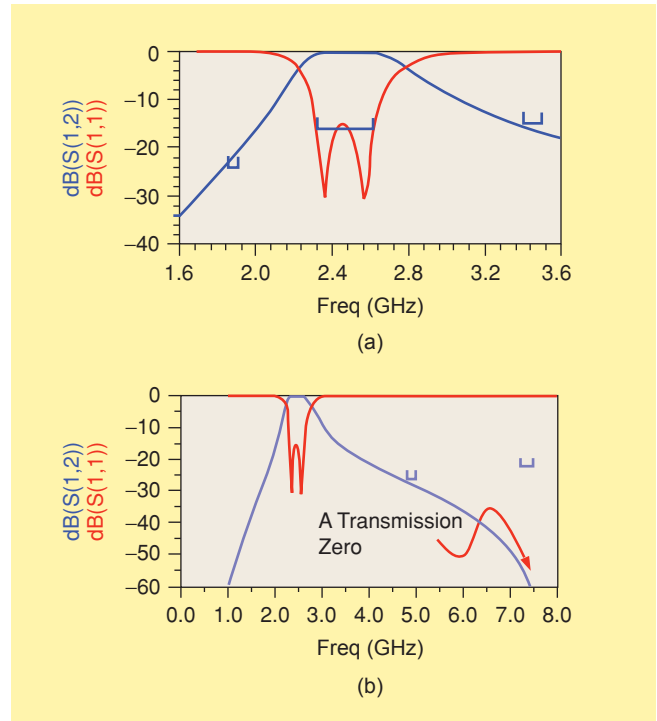


Figure 11. The simulated S-parameter for the optimized filter circuit.

certain layout limitations. The negative capacitors should be absorbed into the capacitor C_r so that we have $C'_r = C_r - C_{12} - C'_{23} = 2.12$ pF. Therefore, we have a complete initial circuit with

- $C_{01} = 1.05$ pF
- $C_{12} = 0.72$ pF
- $C_{23} = 1.05$ pF
- $C'_r = 2.12$ pF
- $\theta = 29.2^\circ$.

It is expected that the responses of this initial filter will not meet all specifications, especially the high-frequency attenuation. The circuit is thus necessary to be further optimized for a better filtering performance. For the optimization, we have included a rough guessed value for the parasitic inductance L_s of 0.18 nH. This may need to be changed later on in the design process. The optimized values obtained from a gradient-based circuit optimizer are

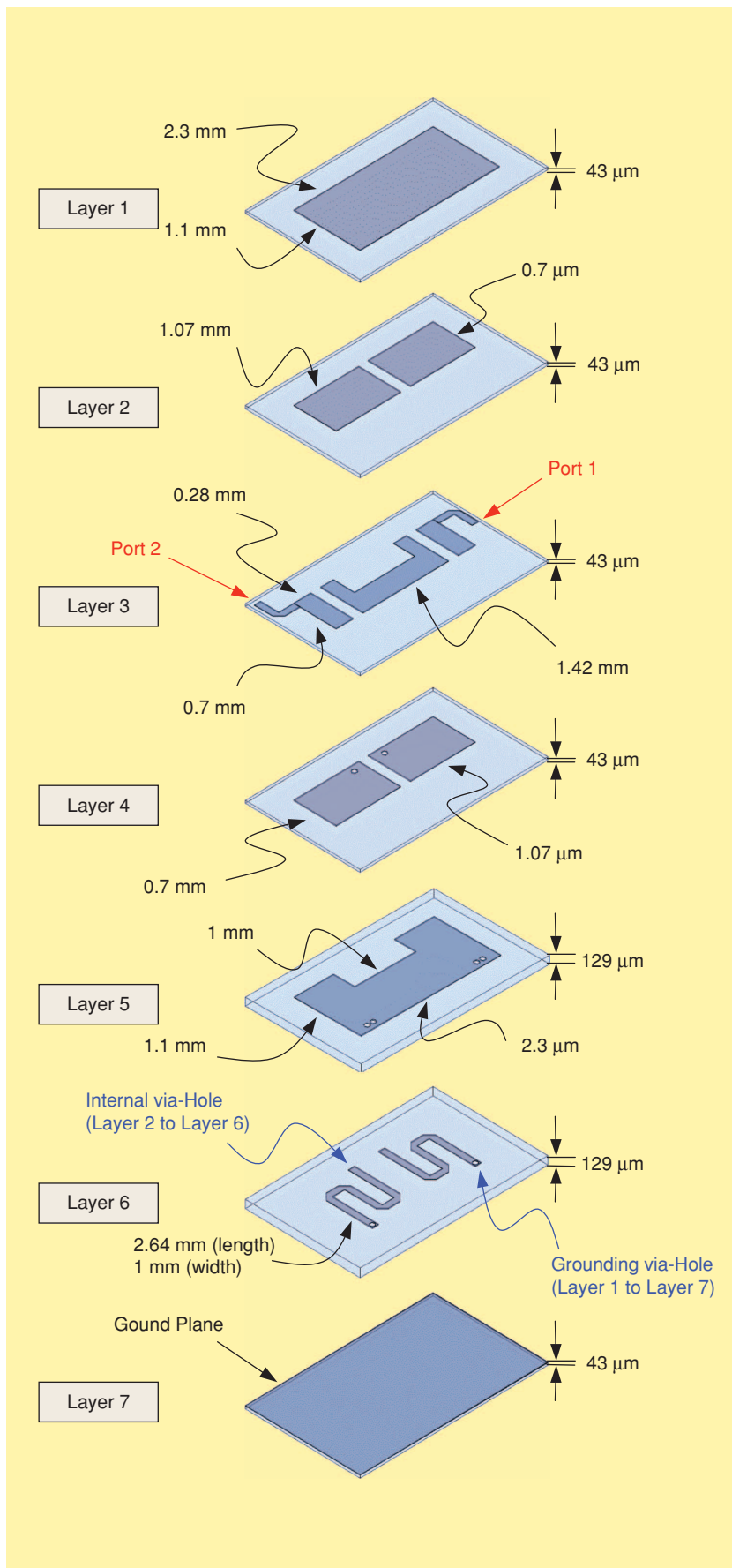


Figure 12. Decomposed layers for the proposed bandpass filter.

- $C_{01} = 1.10 \text{ pF}$
- $C_{12} = 0.65 \text{ pF}$
- $C_{23} = 1.10 \text{ pF}$
- $C'_r = 2.28 \text{ pF}$
- $\theta = 27.7^\circ$
- $L_s = 0.18 \text{ nH}$.

The simulated responses of this optimized filter are shown in Figure 11. From these results, it can be seen that the optimized filter meets all the specifications. It has around a 300-MHz bandwidth of 16-dB return loss. Notice that at 1,850–1,910 MHz, the attenuation barely reaches 24 dB. Nevertheless, if loss is included, the attenuation would definitely be larger.

Once the filter schematic has been obtained, we can start designing the layout. The vertical structure of the substrate should first be determined by specifying how many layers are going to be used and their corresponding thickness. Figure 12 and Figure 13 depict the decomposed as well as complete views for the filter physical layout. In Figure 13, the diagram in the top-left corner gives the grounding structure of the filter. It consists of three conductor plates at three different layers connecting through multiple via holes. The structure in the top-right corner is the two resonators. The meandered lines are sandwiched between the bottom two ground planes to form two striplines (or inductors). Moreover, each line is loaded with a capacitor at one of its ends. Their other ends are grounded through the use of via holes. Coupling capacitors, shown on the bottom-left, are implemented by three conducting plates sandwiched between the two conductors of the loading capacitors. Finally, the complete structure is shown on the bottom-right.

The initial layout is derived from the previously calculated component values with the capacitors' dimensions estimated by the parallel-plate formula. Dimensions for the striplines are directly translated from the electrical parameters Z_0 and θ using a computer program. The final layout is obtained after a few tuning steps using a commercially available EM solver. The tuning is carried out through the so-called space-mapping technique [20], which, in essence, uses a coarse model to provide parameter adjustment guidelines in each tuning step. The resulting filter has an overall size of 1.1 mm × 2.3 mm with a

total of ten dielectric layers with a dielectric constant of 7.8. Simulation results are shown in Figure 14, which shows that the filter meets all the specifications but with a major down-shift of the transmission zero. This is the consequence of underestimating the parasitic inductance. Experimental measurements of a prototype are also plotted in Figure 14.

Conclusions

Over the past few years, a great amount of effort has been spent on LTCC filters or related research [21]–[28]. Some of these components have more advanced functionalities, such as a combination of filter and balun, or a complete front-end module with balun, filter, and matching network. At the same time, advanced methodologies have also been developed to design these components [29]. All the enjoyment of miniaturized RF components or modules is due to the promising three-dimensional design flexibility of LTCC technology. It is expected that a variety of functionally complex components will be continuously available on the market such that the cost and size of the overall wireless terminal can be further reduced.

Various aspects of designing miniaturized LTCC LC filters have been briefly discussed here. Conventional coupled LC resonators are commonly used in LTCC filters for RF applications because of their compact size advantage. The shunted parallel resonator in this type of filter can be realized directly as a lumped-element or distributed quarter-wavelength stripline with or without loaded capacitors. Filters with distributed resonators in general have better passband insertion loss performance. Moreover, there are many ways to improve the rejection performance in an LTCC filter design; for example, by modifying the resonators or admittance inverters so as to introduce transmission zeros at the stopband. It was demonstrated, through a design example, that by making use of the flexibility of LTCC technology, a compact LC bandpass filter can be realized for various RF applications.

References

- [1] R. Kulke, V. Wahle, D. Sollbach, P. Uhlig, M. Rittweger, S. Schmitz, and P. Waldow, "High level of integration for Bluetooth modules on LTCC," in *Proc. IMAPS-Europe Microwave Packaging Conf.*, Friedrichshafen, Germany, June 2003, pp. 16, 23–25 [CD-ROM].
- [2] C. Lee, A. Sutono, C. Lee, S. Han, K. Lim, S. Pinel, E. Tentzeris, and J. Laskar, "A compact LTCC-based Ku-band transmitter module," *IEEE Trans. Adv. Packag.*, vol. 25, pp. 374–384, Aug. 2002.
- [3] S. Chakraborty, K. Lim, A. Sutono, E. Chen, S. Yoo, A. Obatoyinbo, and J. Laskar, "Development of an integrated Bluetooth RF transceiver module using multi-layer system on package technology," in *Proc. IEEE Radio and Wireless Conf.*, Aug. 2001, pp. 117–120.
- [4] L.K. Yeung, J. Wang, Y. Huang, S.-C. Lee, and K.-L. Wu, "Development of an integrated LTCC Bluetooth module," in *Proc. IEEE Asia-Pacific Microwave Conf.*, Dec. 2005, [CD-ROM]. pp 1–4.
- [5] D.W. Lew, J.S. Park, D. Ahn, N.K. Kang, C.S. Yoo, and J.B. Lim, "A design of ceramic chip balun using multilayer configuration," *IEEE Trans. Microwave Theory Tech.*, vol. 49, no. 1, pp. 220–224, Jan. 2001.
- [6] Y. Fujiki, H. Mandai, and T. Morikawa, "Chip type spiral broadside-coupled directional couplers and baluns using low temperature co-fired ceramic," in *Proc. IEEE Electronic Comp. Tech. Conf.*, San Diego, CA, June 1999, pp. 105–110.
- [7] L.K. Yeung and K.-L. Wu, "A compact second-order LTCC bandpass filter with two finite transmission zeros," *IEEE Trans. Microwave Theory Tech.*, vol. 51, no. 2, pp. 337–341, Feb. 2003.

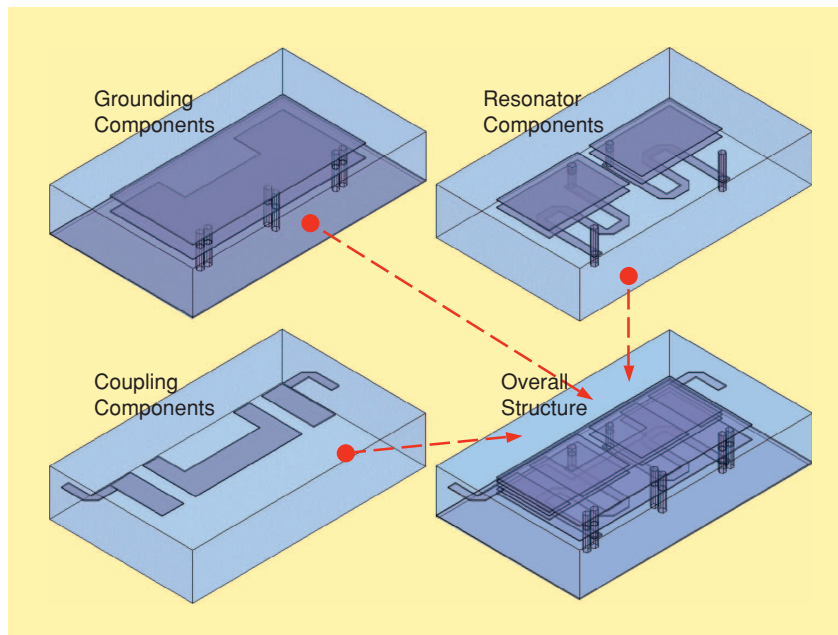


Figure 13. The proposed filter physical structure.

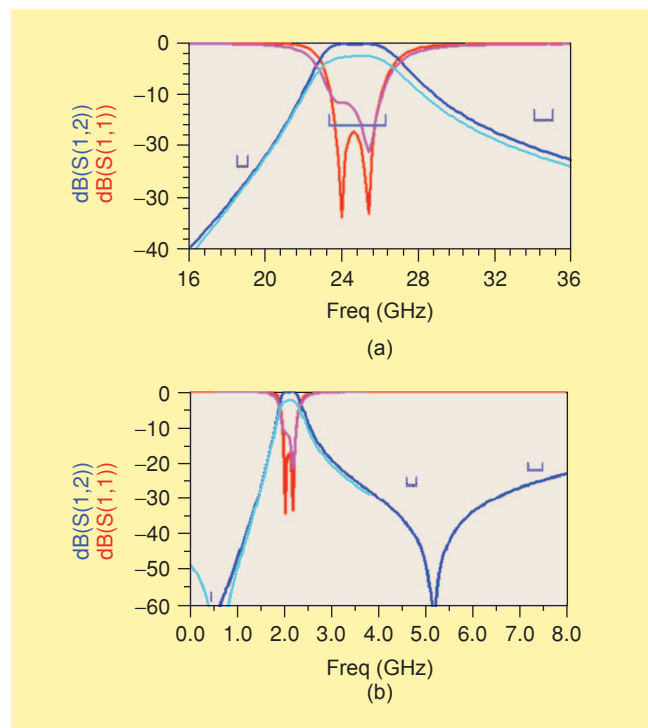



Figure 14. The EM simulated and measured S-parameter for the physical layout.

- [8] A. Sutono, J. Laskar, and W. Smith, "Development of integrated three dimensional Bluetooth image reject filter," in *IEEE MTT-S Int. Microwave Symp. Dig.*, June 2000, pp. 339–342.
- [9] V. Piatnitsa, E. Jakku, and S. Leppaevuori, "Design of a 2-pole LTCC filter for wireless communications," *IEEE Trans. Wireless Comm.*, vol. 3, pp. 379–381, Mar. 2004.
- [10] C.W. Tang, Y.C. Lin, and C.Y. Chang, "Realization of transmission zeros in combine filters using an auxiliary inductively coupled ground plane," *IEEE Trans. Microwave Theory Tech.*, vol. 51, no. 10, pp. 2112–2118, Oct. 2003.
- [11] J.W. Sheen, "LTCC-MLC duplexer for DCS-1800," *IEEE Trans. Microwave Theory Tech.*, vol. 47, pp. 1883–1890, Sept. 1999.
- [12] M.C. Park, B.H. Lee, and D.S. Park, "A laminated balance filter using LTCC technology," in *Proc. IEEE Asia-Pacific Microwave Conf.*, Dec. 2005, [CD-ROM], pp. 1–4.
- [13] L.K. Yeung and K.-L. Wu, "An LTCC balanced-to-unbalanced extracted-pole bandpass filter with complex load," *IEEE Trans. Microwave Theory Tech.*, vol. 54, no. 4, pp. 1512–1518, Apr. 2006.
- [14] G.L. Matthaei, L. Young, and E.M.T. Jones, *Microwave Filters, Impedance Matching Networks and Coupling Structures*. New York: McGraw-Hill, 1980.
- [15] W.Y. Leung, K.K. Cheng, and K.-L. Wu, "Multilayer LTCC bandpass filter design with enhanced stopband characteristics," *IEEE Microwave Wireless Comp. Lett.*, vol. 12, no. 7, pp. 240–242, July 2002.
- [16] C.W. Tang, "Harmonic-suppression LTCC filter with the step-impedance quarter-wavelength open stub," *IEEE Trans. Microwave Theory Tech.*, vol. 52, no. 2, pp. 617–624, Feb. 2004.
- [17] Y.H. Jeng, S.F. Chang, and H.K. Lin, "A high stopband-rejection LTCC filter with multiple transmission zeros," *IEEE Trans. Microwave Theory Tech.*, vol. 54, no. 2, pp. 633–638, Feb. 2006.
- [18] M. Sagawa, M. Makimoto, and S. Yamashita, "Geometrical structures and fundamental characteristics of microwave stepped-impedance resonators," *IEEE Trans. Microwave Theory Tech.*, vol. 45, no. 7, pp. 1078–1085, July 1997.
- [19] C. Hoer and C. Love, "Exact inductance equations for rectangular conductors with applications to more complicated geometries," *J. Res. Natl. Bur. Stand. - C, Eng. Instrum.*, vol. 69C, no. 2, pp. 127–137, Apr.–June 1965.
- [20] K.-L. Wu, R. Zhang, M. Ehlert, and D.G. Fang, "An explicit knowledge-embedded spacing mapping technique and its application to optimization of LTCC RF passive circuits," *IEEE Trans. Microwave Theory Tech.*, vol. 26, no. 2, pp. 399–406, June 2003.
- [21] K. Kageyama, K. Saito, H. Murase, H. Utaki, and T. Yamamoto, "Tunable active filters having multilayer structure using LTCC," *IEEE Trans. Microwave Theory Tech.*, vol. 49, no. 12, pp. 2421–2424, Dec. 2001.
- [22] V. Piatnitsa, E. Jakku, and S. Leppaevuori, "Design of a 2-pole LTCC filter for wireless communications," *IEEE Trans. Wireless Communications*, vol. 3, no. 2, pp. 379–381, Mar. 2004.
- [23] G. Wang, M. Van, F. Barlow, and A. Elshabini, "An interdigital bandpass filter embedded in LTCC for 5-GHz wireless LAN applications," *IEEE Microwave Wireless Comp. Lett.*, vol. 15, no. 5, pp. 357–359, May 2005.
- [24] K. Rambabu and J. Bornemann, "Simplified analysis technique for the initial design of LTCC filters with all-capacitive coupling," *IEEE Trans. Microwave Theory Tech.*, vol. 53, no. 5, pp. 1787–1791, May 2005.
- [25] C. Chang and S. Chung, "Bandpass filter of serial configuration with two finite transmission zeros using LTCC technology," *IEEE Trans. Microwave Theory Tech.*, vol. 53, no. 7, pp. 2383–2388, July 2005.
- [26] W. Tung, Y. Chiang, and J. Cheng, "A new compact LTCC bandpass filter using negative coupling," *IEEE Microwave Wireless Comp. Lett.*, vol. 15, no. 10, pp. 641–643, Oct. 2005.
- [27] Y. Jeng, S. Chang, and H. Lin, "A high stopband-rejection LTCC filter with multiple transmission zeros," *IEEE Trans. Microwave Theory Tech.*, vol. 54, no. 2, pp. 633–638, Feb. 2006.
- [28] K. Lin, C. Chang, M. Wu, and S. Chung, "Dual-bandpass filters with serial configuration using LTCC technology," *IEEE Trans. Microwave Theory Tech.*, vol. 54, no. 6, pp. 2321–2328, June 2006.
- [29] C.W. Tang and S.F. You, "Design methodologies of LTCC bandpass filters, diplexer and triplexer with transmission zeros," *IEEE Trans. Microwave Theory Tech.*, vol. 54, no. 2, pp. 717–723, Feb. 2006. 

Fall 2008 ARFTG Microwave Measurement Symposium



www.arftg.org

Conference, Short Course, Two Workshops and a User Forum

9–12 December 2008

Red Lion Jantzen Beach Hotel, Portland, Oregon, USA

Digital Object Identifier 10.1109/MMM.2008.929676